27.5 km$^2$. The thickness of the flows is quite variable but is generally not closely determinable except near their margins. Near their sources, the flows reach thicknesses of about 30 m; surface relief on the larger flows locally approaches 10 m. If one assumes an average flow thickness of 10 m, probably a reasonable approximation, the minimum volume of the postglacial lavas is 0.25 km$^3$. However, the total areal extent of the larger flows is not known with certainty, and, because estimates of mean thickness are based on few exposed sections, the actual volume may be somewhat greater.

Radiocarbon determinations of six charcoal samples collected near the top of the Humuula paleosol at widely separated localities provide limiting ages for the Holocene eruptions on the south slope of the mountain and record the end of the Humuula soil-forming interval (Table 1). Within the statistical limits of error, the small difference in age between samples that lay directly beneath Puu Kole tephra, Puu Kole lava, and Puu Loaloa tephra suggests that the entire volcanic succession resting on the paleosol was erupted within a brief interval of probably no more than several hundred years. This conclusion is supported by the absence of weathering horizons between the top of the Humuula paleosol and the modern surface soil. If the entire succession represents a single eruptive episode, the outcrop pattern and stratigraphic relationships indicate that the vents must have opened progressively downslope, a phenomenon common to historic eruptions on the island (*6*). An upper limiting date of 845±95 years for Puu Loaloa tephra, obtained from charcoal at the base of the modern solum, may postdate the eruption of the underlying tephra by a considerable span of time.

Radiocarbon dates were obtained for algal sediments from the bottom of Lake Waiau, a shallow body of water at 3970-m altitude which lies within the glaciated area (*7*). These dates indicate that the summit ice cap must have largely disappeared by about 10,000 years ago. The Humuula soil-forming interval terminated some 5500 years later in those areas mantled by postglacial volcanics. Therefore, the top of the buried Humuula paleosol lies temporally above the boundary between the Middle and Upper Members of the Laupahoehoe Series. In areas unaffected by Holocene volcanism, soil formation presumably has continued uninterrupted to the present. In comparison with the Humuula paleosol, soil developed on the postglacial lavas and tephra sheets during the past 4500 years is thinner and has weaker profile characteristics.

A layer of dark ash approximately 4500 years old was noted in a sediment core taken from Lake Waiau (*8*). The layer, formed by several separate ash falls, lies 1.5 m below the top of the core and consists of particles as large as 1 mm in diameter. The ash was attributed to an eruption of a nearby cone (*8*), but all cinder cones lying inside the 3700-m contour (within 3 km of Lake Waiau) are Pleistocene in age; therefore, the ash may have originated in one or more of the major pyroclastic eruptions on the south slope of the mountain (Puu Kole or Puu Loaloa), which also occurred about 4500 years ago. The grain size and thickness of the ash in the lake sediments apparently are consistent with such a distant source. A layer of similar dark-gray ash, 15 cm thick, was found overlying Makanaka drift in shallow soil pits excavated 1.5 km northwest of Summit Cone at an altitude of 4040 m. Dark-gray ash also was encountered in the vicinity of Pohakuloa State Park in the Mauna Kea–Mauna Loa saddle, where it blankets the surface of a Makanaka outwash fan. A layer of finer dark ash, as much as 4 cm thick and underlying 50 cm of alluvium, occurs near the surface of a fan at the west end of the U.S. Army Pohakuloa Training Area, some 3 km farther west. If these separate ash occurrences all represent the same eruptive event (or events), the mid-Holocene tephra blanket must originally have covered an area of at least 250 km$^2$, which would make it a widespread and useful stratigraphic marker horizon across the upper slopes of the volcano.

STEPHEN C. PORTER
*Department of Geological Sciences, University of Washington, Seattle 98105*

### References and Notes

1. H. E. Gregory and C. K. Wentworth, *Geol. Soc. Amer. Bull.* **48**, 1719 (1937); C. K. Wentworth and W. E. Powers, *ibid.* **52**, 1193 (1941); H. T. Stearns, *ibid.* **56**, 267 (1945).
2. Tephra is a collective term for all air-deposited pyroclastic sediments ejected from a volcanic vent during an eruption. It includes volcanic dust, ash, cinders, lapilli, scoria, pumice, bombs, and blocks.
3. H. T. Stearns and G. A. Macdonald, *Hawaii Div. Hydrogr. Bull.* **9** (1946).
4. Kipukas are island-like areas of older land surrounded by later lava flows.
5. G. D. Fraser, *U.S. Geol. Surv. Prof. Pap. 400-B* (1960), p. B354.
6. G. A. Macdonald and A. T. Abbott, *Volcanoes in the Sea* (Univ. of Hawaii, Honolulu, 1970), p. 50.
7. J. D. Buckley and E. H. Willis, *Radiocarbon* **11**, 53 (1969).
8. A. H. Woodcock, M. Rubin, R. A. Duce, *Science* **154**, 647 (1966).
9. Supported by NSF grant GA-20320. I thank G. A. Macdonald for reviewing a draft of this paper.

20 January 1971

## Theoretical and Experimental Basis for a Specific Countertransport System in Membranes

Abstract. *A sodium ion carrier transport system contains the antibiotic monensin in the membrane and uses a pH gradient as an energy source. The experimental results are in accord with theoretical predictions based on a mechanism which is understood on a molecular level.*

Our experiments demonstrate the selective transport of sodium ions across a membrane. The membrane contains a carrier that reacts selectively with a sodium ion and transports the ion across the membrane against its own concentration gradient. The energy source for this transport comes from the simultaneous diffusion of a second solute. The results represent an example of coupled facilitated diffusion similar to the oxygen–carbon monoxide system reported earlier (*1*). In these systems, solute fluxes can be coupled hundreds of times more strongly than in conventional multicomponent diffusion. Such membranes should find major industrial applications in specific chemical separations and in pollution control, and they should provide convenient biological analogs for the membranes found in living systems.

The main feature of the mechanism is that the carrier reacts competitively with both the solute being transported against its own gradient and with a second solute supplying the necessary energy. The mechanism by which this membrane functions is understood explicitly on a molecular level and includes consideration of reaction and diffusion of all species within the membrane. Whereas our discussion is primarily concerned with a specific mem-

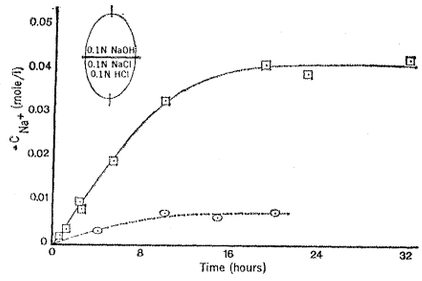


Fig. 1. Difference in sodium ion concentration across the membrane as a result of countertransport: membrane containing a saturated hexanol solution of monensin (solid line); membrane containing hexanol only (dashed line).

brane, the results are easily generalized since the chemical requirements for effective countertransport are not as stringent as might have been anticipated. A mechanism by which the specific contaminants, such as mercury, are concentrated by living organisms may also be visualized within this framework.

For the experiment, the sodium concentration difference across the membrane resulting from countertransport is shown as a function of time in Fig. 1. The apparatus consists of two well-stirred solutions separated by a membrane containing a hexanol solution of the antibiotic monensin (*2*). The initial concentrations of electrolytes in these two solutions are shown in Fig. 1 for a typical series of experiments. The two curves show the effect of monensin on sodium ion transport. The upper curve gives data for a membrane containing a saturated hexanol solution of monensin. The concentration difference of sodium ion, which is initially zero, increases to almost 50 percent of the average sodium ion concentration. The lower curve, which gives data for a membrane containing hexanol alone, shows a much smaller concentration diffusion arising from multicomponent diffusion effects. Previous experiments with monensin and similar compounds have not generated concentration differences larger than this lower curve; they have never shown effects that could not be attributed to multicomponent diffusion (*3*).

Our results are in accord with theoretical predictions based on two assumptions (*4*). (i) The carrier is assumed to react so rapidly with the solutes being transported that the thickness of the reaction zone is much less than the overall thickness of the membrane; that is, the second Damkohler number is greater than 10 (*5*). (ii) All species are assumed to have the same diffusion coefficient, $D$; while this restriction is easily removed, it greatly simplifies the algebraic form of the results. The total steady state flux, $j_1$, of species "1" is found to be

$$-j_1 = \frac{Dk_1}{l}(C_{1B} - C_{1A}) \quad \text{(ordinary diffusion)}$$

$$+\frac{Dk_1}{l}[R(1 + k_2K_2\bar{C}_2)](C_{1B} - C_{1A}) \quad \text{(facilitated diffusion)}$$

$$-\frac{Dk_1}{l}[R\,k_2K_2\bar{C}_1](C_{2B} - C_{2A}) \quad \text{(coupled transport)}$$

where $D$ is the diffusion coefficient of all species, $k_i$ is the distribution coefficient between solution and membrane, $K_i$ is the equilibrium constant for the carrier reaction, $l$ is the membrane thickness, $\bar{C}_i$ is the average concentration of species "i," and $(C_{iB} - C_{iA})$ is the concentration difference of solute "i" across the membrane. The quantity $R$ is equal to

$$K_1\bar{C}/[(1 + k_1K_1C_{1A} + k_2K_2C_{2A}) \times (1 + k_1K_1C_{1B} + k_2K_2C_{2B})]$$

where $\bar{C}$ is the sum of complex and uncomplexed carrier concentration. The first term on the right-hand side of the flux equation represents the fluxes due to ordinary diffusion. The second term is similar to that for "facilitated" diffusion resulting from a single carrier reaction. For example, this term describes the augmented diffusion of oxygen by hemoglobin (*6*). The last term on the right-hand side represents the flux of species "1" engendered by the two competitive carrier-solute reactions. It is this term that is responsible for the coupled transport effects observed here.

For the specific carrier studied, the phenomena described by this equation are shown in Fig. 2. Monensin and sodium ion form a complex at high $p$H, so that there is a clathrate-like structure around the ion (step 1). After the slow diffusion (step 2), protonation causes a conformational change that results in the release of previously complexed sodium ion (step 3). The diffusion of the protonated monensin completes the cycle (step 4). The sodium flux arising from its own concentration gradient (step 5), which opposes the countertransport, is small because of the low solubility of this ion within the membrane ($k_1$ small). This figure is an oversimplification since it neglects the fact that the reaction between sodium ion and monensin occurs at all points in the membrane and not just at the surfaces. However, this

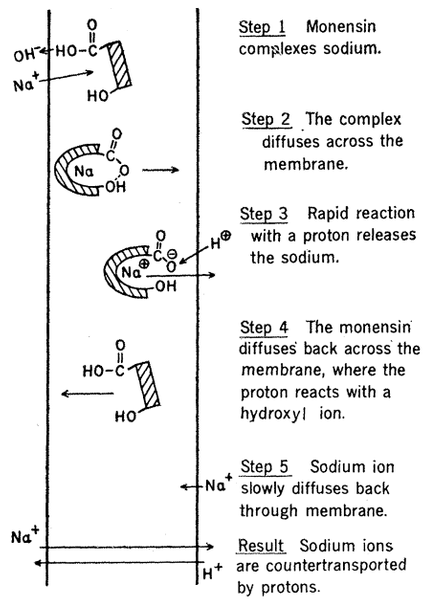


Fig. 2. A simplified mechanism for sodium ion countertransport.

figure is included because it aids in understanding this phenomenon. The important aspects of this mechanism are that the solute which supplies the energy (in this case $H^+$) always diffuses in the same direction as its concentration gradient, and that the complex by means of which countertransport is achieved (in this case, the sodium monensin complex) also diffuses in the same direction as its concentration gradient. It is the coupling of these two diffusion fluxes which causes the sodium ion transport and results in sodium ion being moved against its concentration gradient. This effect is predicted to be large if $k_1K_1$ and $k_2K_2$ are large and if complex diffusion (step 2) is greater than back diffusion (step 5) (*4*). The symmetrical form of this equation also predicts the opposite phenomena; that is, a sodium ion flux will generate a $p$H difference.

The predictions of the equation presented above and of the mechanism shown (Fig. 2) are in accord with the experimental results. As is shown in Fig. 1, the sodium ion concentration difference increases rapidly because of the action of the carrier (steps 1 to 4, Fig. 2). This difference is found experimentally to increase until the $p$H difference across the membrane disappears, as predicted by the equation. After this point is reached, the concentration difference of sodium ion decreases slowly because sodium ion in its uncomplexed form is only slightly soluble in the membrane. In addition, the amount of coupled transport has

been found to be directly proportional to the amount of carrier, as is predicted.

If membranes based on this mechanism are used with more than two solutes, they may exhibit selective countertransport, separating and concentrating one of the ions. We have made experiments using monensin-containing membranes which show the selective countertransport of sodium ion in the presence of potassium ion. The data are very similar to those of Fig. 1, with the maximum sodium concentration difference about three times larger than the maximum concentration difference observed for potassium.

For the simultaneous transport of several solutes against this concentration gradient, the chemical requirements on the carrier are not stringent. If a *p*H gradient is the energy source, cations may be moved against this gradient with any weak acid as a carrier, and the anions with any weak base as a carrier. In addition, the energy source for this effect is not limited to acid-base reactions, but can, in principle, be applied to any diffusional process that can be coupled via the carrier to the solute being transported. We have observed such nonselective effects with membranes containing octanol or trichloroethane solutions of silicones. Others have reported similar nonspecific membranes which employ pentanol solutions of stearic acid (*7*) or aqueous acetate solutions (*8*). However, because of an inadequate theoretical basis, the interpretation of previous experiments has often been uncertain.

E. L. CUSSLER
*Department of Chemical Engineering, Carnegie-Mellon Institute, Pittsburgh, Pennsylvania 15213*
D. FENNELL EVANS
*Department of Chemistry, Case Western Reserve University, Cleveland, Ohio 44106*
SISTER M. A. MATESICH
*Department of Chemistry, Ohio Dominican College, Columbus, Ohio*

### References and Notes

1. M. Mochizuki and R. E. Forster, *Science* **138**, 897 (1962); R. C. La Force, *Trans. Faraday Soc.* **62**, 1458 (1966).
2. J. W. Chamberlin and A. Agtarap, *Org. Mass Spectrom.* **3**, 271 (1970).
3. R. Ashton and L. K. Steinrauf, *J. Mol. Biol.* **49**, 547 (1970).
4. E. L. Cussler, in preparation.
5. J. D. Goddard, J. S. Shultz, R. J. Bassett, *Chem. Eng. Sci.* **25**, 665 (1970).
6. K. H. Keller and S. K. Friedlander, *J. Gen. Physiol.* **49**, 663 (1966).
7. J. H. Moore and R. S. Schecter, *Nature* **222**, 476 (1969).
8. R. Patterson, *ibid.* **217**, 545 (1968).
9. Supported by NIH, AM GM 13685-01, and the Office of Saline Water grant 14-30-2615.

22 October 1970; revised 21 December 1970

# Ornithine Decarboxylase Stimulation in Rat Ovary by Luteinizing Hormone

Abstract. *In normal albino rats with a 4-day estrous cycle, the activity of ovarian ornithine decarboxylase undergoes a transitory rise on the evening of proestrus and only at that time. The response could be elicited by the administration of either luteinizing hormone or human chorionic gonadotrophin. When antiserum to luteinizing hormone was injected at 2 p.m. on the day of proestrus, the induction of ornithine decarboxylase was blocked, an indication that the enzyme is under luteinizing hormone control. The strategic positioning of the induction of ornithine decarboxylase between the normal release of luteinizing hormone and ovulation implies that putrescine is associated with the ovulatory process, and opens a new avenue of research on the control of ovulation.*

Mammalian ornithine decarboxylase is a key enzyme in the biosynthesis of the polyamines, spermine and spermidine (*1*, *2*). It responds rapidly to various stimuli, and high levels of the enzyme occur in the rat liver after partial hepatectomy (*1–3*) or after the administration of growth hormone (*4*). In the ventral prostate of rat, testosterone regulates ornithine decarboxylase activity (*5*); and we now report on the possible role of polyamines in female reproductive physiology.

Female Sprague-Dawley rats (150 to 180 g) were followed through three consecutive estrous cycles. Each was killed at 10 a.m., 2 p.m., or 8 p.m., at the stage of the estrous cycle indicated. Ornithine decarboxylase activity of the ovaries was assayed as described by Russell and Snyder (*2*), except that the reaction was carried out in Warburg vessels and the evolved carbon dioxide was trapped on Hyamine-impregnated filter paper (*6*). The specific activity of the DL-[1-$^{14}$C]ornithine used was 1 mc/mmole. The assay medium contained 100 mg of homogenized tissue, 0.2 $\mu$mole of DL-[1-$^{14}$C]ornithine, 0.2 $\mu$mole of pyridoxal phosphate in 0.1*M* phosphate buffer, *p*H 7.2, in a final volume of 2 ml. The incubation time was 30 minutes at 37°C in air. The reaction was stopped with 0.2 ml of 1*M* citric acid injected through a rubber septum and shaken for an additional 30 minutes. The filter paper was transferred to a glass vial containing 3 ml of ethanol and 7 ml of toluene [0.4 percent of 2,4-diphenyloxazole and 0.01 percent of *p*-bis-(*O*-methylstyryl)benzene] and assayed for radioactivity in a liquid scintillation spectrometer. The amount (90 percent) of $^{14}CO_2$ from [1-$^{14}$C]ornithine was nearly equivalent to that obtained as [$^{14}$C]putrescine from [5-$^{14}$C]ornithine.

The characteristic feature of ornithine decarboxylase of the ovary was the pronounced transitory rise in enzyme activity which occurred only on the evening of proestrus (Fig. 1). A more detailed study of the development of ornithine decarboxylase activity during late proestrus verified this pattern of enzyme activity and showed that the major increase in enzyme activity occurred between 5 and 8 p.m. and was nearly normal by 10 p.m. (Fig. 2). A similar study of the other periods of the estrous cycle did not reveal any significant change in ornithine decarboxylase activity. The unique timing of this rise in ornithine decarboxylase in the ovary leads us to suspect that this enzyme may be under hormonal control.

In cycling female albino rats, lutein-

Table 1. Effect of hormonal treatment on ornithine decarboxylase activity in rat ovary. Animals in proestrus were injected subcutaneously with the designated hormone at 9 a.m. on the morning of proestrus, and the ornithine decarboxylase in the ovary was determined 4 hours later. The number of animals is shown in parentheses. Activity is expressed as the number (± S.E.) of nanomoles of $CO_2$ formed per gram of tissue per hour.

| Hormone | Dose (per kg) | Ornithine decarboxylase activity (nmole $g^{-1}$ $hr^{-1}$) |
|---|---|---|
| None | None | 4.15 ± 0.63 (6) |
| LH | 100 $\mu$g | 37.78 ± 3.55 (6) |
| HCG | 50 units | 46.65 ± 5.78 (9) |
| Estradiol | 1 mg | 4.38 ± 0.98 (6) |
| Progesterone | 5 mg | 4.98 ± 0.98 (6) |
| Thyroxine | 2 mg | 2.43 ± 0.75 (3) |
| Testosterone | 50 mg | 7.40 ± 4.98 (3) |
| FSH | 25 units | 7.65 ± 3.93 (6) |

Table 2. Inhibition of the induction of ornithine decarboxylase in rat ovary by bovine antiserum to luteinizing hormone. The enzyme activity is expressed as nanomoles (± S.E.) of $CO_2$ formed per gram of tissue per hour.

| Treatment | Ornithine decarboxylase activity (nmole $g^{-1}$ $hr^{-1}$) |
|---|---|
| Proestrus 2 p.m. | 5.43 ± 1.35 (3) |
| Proestrus 7 p.m. | 29.70 ± 13.43 (3) |
| Proestrus 7 p.m.* | 2.03 ± 0.73 (3) |

* Injected with antiserum (0.3 ml) intraperitoneally at 2 p.m.